

The Information Content of Anisotropic Baryon Acoustic Oscillation Scale Measurements

Ashley J. Ross^{*1,2}, Will J. Percival², Marc Manera^{3,2}

¹Center for Cosmology and AstroParticle Physics, The Ohio State University, Columbus, OH 43210, USA

²Institute of Cosmology & Gravitation, Dennis Sciama Building, University of Portsmouth, Portsmouth, PO1 3FX, UK

³University College London, Gower Street, London WC1E 6BT, UK

Accepted by MNRAS

ABSTRACT

Anisotropic measurements of the Baryon Acoustic Oscillation (BAO) feature within a galaxy survey enable joint inference about the Hubble parameter $H(z)$ and angular diameter distance $D_A(z)$. These measurements are typically obtained from moments of the measured 2-point clustering statistics, with respect to the cosine of the angle to the line of sight μ . The position of the BAO features in each moment depends on a combination of $D_A(z)$ and $H(z)$, and measuring the positions in two or more moments breaks this parameter degeneracy. We derive analytic formulae for the parameter combinations measured from moments given by Legendre polynomials, power laws and top-hat Wedges in μ , showing explicitly what is being measured by each in real-space for both the correlation function and power spectrum, and in redshift-space for the power spectrum. The large volume covered by modern galaxy samples means that the correlation function can be well approximated as having no correlations at different μ on the BAO scale, and that the errors on this scale are approximately independent of μ . Using these approximations, we derive the information content of various moments. We show that measurements made using either the monopole and quadrupole, or the monopole and μ^2 power-law moment, are optimal for anisotropic BAO measurements, in that they contain all of the available information using two moments, the minimal number required to measure both $H(z)$ and $D_A(z)$. We test our predictions using 600 mock galaxy samples, matched to the SDSS-III Baryon Oscillation Spectroscopic Survey CMASS sample, finding a good match to our analytic predictions. Our results should enable the optimal extraction of information from future galaxy surveys such as eBOSS, DESI and Euclid.

Key words: cosmology: observations - (cosmology:) large-scale structure of Universe

1 INTRODUCTION

The clustering of galaxies contains the imprint of the BAO scale, at a fixed co-moving distance ~ 150 Mpc (see, e.g., Eisenstein 2005 for a review). The apparent location of the position of the feature along the line of sight (los) depends on the value of the Hubble parameter, $H(z)$, and its apparent location transverse to the los depends on the angular diameter distance, $D_A(z)$. Thus, measurements of the clustering of galaxies along and transverse to the los allows simultaneous measurement of $D_A(z)$ and $H(z)$ (see, e.g., Hu & Haiman 2003 and Padmanabhan & White 2008).

The Sloan Digital Sky Survey (SDSS; York et al. 2000) III (Eisenstein et al. 2011) Baryon Oscillation Spectroscopic Survey (BOSS; Dawson et al. 2013) has provided galaxy samples large enough to robustly measure BAO scale information along and transverse to the los and thus independently measure $D_A(z)$ and

$H(z)$. Two methods have been applied to BOSS data that isolate the BAO information: “Wedges” (Kazin et al. 2012, 2013) and “Multipoles” (Xu et al. 2013) and results using both methodologies are presented in Anderson et al. (2014).

As measurements become statistically more precise, there is an increased pressure on the analysis pipeline to ensure the extraction of information is robust. The elements of the pipeline requiring careful consideration include the models to be fitted to the data, the statistical procedure to be applied, accurate estimation of systematic errors, and a precise knowledge of what is actually being measured. In this paper, we focus on the latter issue for anisotropic BAO measurements, considering the information content of moments of 2-point statistics. Recently, studies such as Taruya et al. (2011); Font-Ribera et al. (2014); Blazek et al. (2014) have also studied the information content of anisotropic clustering measurements. In our study, we build on these results by focusing purely on the $D_A(z)$ and $H(z)$ information that can be measured via the BAO position, thereby enabling an alternative and simplified analytic treat-

* Email: ross.1333@osu.edu; Ashley.Jacob.Ross@gmail.com

ment. Further, we focus primarily on post-‘reconstruction’ clustering measurements (Eisenstein et al. 2007), where the large-scale clustering amplitudes are expected to be isotropic. In this case, we show that moments based on polynomials of the cosine of the angle to the los (μ) are complete for any non-degenerate set of two moments that includes zero and second order terms. We then compare the precision of $D_A(z)$ and $H(z)$ measurements one obtains using the Wedges and Multipoles methodology, both based on analytical predictions and empirical measurements.

Our paper is structured as follows: After developing general formulae in Section 2, we assume that information is equally distributed with respect to $\mu \equiv \cos(\theta_{\text{los}})$, equivalent to a spherically symmetric distribution and matching empirical results, and in Section 3 we predict the variance and covariance expected on $D_A(z)$ and $H(z)$ measurements for two simple combinations of measurements: one in which a combination of the spherically averaged clustering and clustering averaged over a μ^p window are used, and another using Wedges split at an arbitrary μ_d . In Section 4, we describe how the BAO scale can be fitted using the different methodologies. In Section 5, we measure the BAO scale using 600 mock BOSS samples and compare the results obtained using each methodology, and to the results of Anderson et al. (2014). Where applicable, we assume the same fiducial cosmology as in Anderson et al. (2014): $\Omega_m = 0.274$, $h = 0.7$, $\Omega_b h^2 = 0.0224$.

2 THE ANISOTROPIC BAO SIGNAL

In this section we describe our formalism for considering measurements of the projected BAO scale including an isotropic dilation, and the anisotropic Alcock-Paczynski effect (Alcock & Paczynski 1979). We present our formalism in configuration space, but our derivations are equally valid in Fourier space and therefore applicable to $P(k, \mu)$ measurements.

The observed distance between two galaxies r defined assuming a fiducial or reference cosmological model, and the observed cosine of the angle the pair makes with respect to the line-of-sight (los) μ are given by

$$r^2 = r_{\parallel}^2 + r_{\perp}^2; \quad \mu = \frac{r_{\parallel}}{r}, \quad (1)$$

where r_{\parallel} is the los separation and r_{\perp} is the transverse separation. The estimate of these separations is dependent on the assumed cosmology. Defining

$$\alpha_{\parallel} \equiv H(z)_{\text{fid}}/H(z)_{\text{true}}; \quad \alpha_{\perp} \equiv D_{A,\text{true}}/D_{A,\text{fid}}, \quad (2)$$

the true separation, r' , is given by

$$r' = \alpha r = \sqrt{\alpha_{\parallel}^2 r_{\parallel}^2 + \alpha_{\perp}^2 r_{\perp}^2}. \quad (3)$$

We can re-arrange the above equations to express the stretch as a function of the angle to the line of sight:

$$\alpha(\mu) = \sqrt{\mu^2 \alpha_{\parallel}^2 + (1 - \mu^2) \alpha_{\perp}^2}. \quad (4)$$

Assuming symmetry around $\mu = 0$, we can consider any moment of the 2-point clustering signal as an integral over measurements made along different directions with given μ weighting. For the correlation function we can write

$$\xi_F(r) = \int_0^1 F(\mu) \xi(r, \mu) d\mu, \quad (5)$$

where $F(\mu)$ gives the relative weight of each direction to the moment. For the monopole of the correlation function $\xi_0(r)$, for example, $F(\mu) = 1$. In this paper we only consider functions $F(\mu)$ that are normalised, that is for which $\int_0^1 F(\mu) d\mu = 1$.

In real-space, the correlation function for galaxies in a thin slice in μ can be written $A(\mu)\xi(r'/\alpha(\mu))$, where $A(\mu)$ alters the amplitude, but not the shape or BAO position. If RSD have been removed during a ‘reconstruction’ (Eisenstein et al. 2007) step, this also holds. Pre-reconstruction in redshift space, we need to adjust the template to be fitted to allow for correlation function shape changes (Jeong et al. 2014). If $\alpha \neq 1$, Eq. (5) describes a shift in the mean position of the BAO in the moment, which we denote α_F , together with a ‘broadening’ of the BAO bump, which is now the superposition of $\alpha(\mu)$, which varies as given in Eq. 4. For cosmological models close to the fiducial cosmology used to calculate the correlation function, the broadening is small and is degenerate with the non-linear BAO damping. Consequently information from the BAO feature width is commonly neglected, with the primary measurement being the BAO position α_F . Information from the broadening was included in the anisotropic BAO measurements of Anderson et al. (2014), where models of the moments were calculated by integrating directly over $\xi(r, \mu)$. The additional constraints available from the observed shape of the BAO feature mean that the contours from any single moment in α_{\parallel}^2 and α_{\perp}^2 are closed, but this closure of the contours is not important when fitting to multiple moments, which generally break this degeneracy much more strongly.

We seek to express the expectation for the measured stretch, α_F , determined from a moment of the 2-point clustering signal (ξ_F ; Eq. 5), in terms of the radial and transverse stretch through the expression for $\alpha(\mu)$ given by Eq. 4. Following the arguments above, we assume the information on $\alpha(\mu)$ is separable from the overall shape of the clustering signal. This is equivalent to the modeling used in, e.g., Anderson et al. (2014) BAO fits to the measured $P(k)$, where the model consists of a BAO feature and nuisance parameters describing the overall shape of $P(k)$, and similar to the modeling used to fit $\xi(s)$ in the same study. When this is case, the maximum likelihood $\alpha(\mu)$ determined from any measured $\xi_{\text{meas}}(\mu)$ must be independent of any other parameters. We further assume that information in different μ bins is independent and distributed equally (which we justify empirically in Section 3), and thus the maximum likelihood stretch α_i in any μ bin i are independent. This combination of assumptions implies that, for positive-definite windows $F(\mu)$, the maximum likelihood α_F obtained from $\Sigma_i F(\mu_i) \xi(\mu_i) \Delta\mu_i$ is the same as the weighted sum of individual maximum likelihood α_i , $\Sigma_i F(\mu_i) \alpha_i \Delta\mu_i$, which is

$$\alpha_F = \int_0^1 d\mu F(\mu) [\mu^2 \alpha_{\parallel}^2 + (1 - \mu^2) \alpha_{\perp}^2]^{\frac{1}{2}} \quad (6)$$

for infinitesimal bins in μ and the corresponding ξ_F clustering measurements defined by Eq. 5.

One can fit to $\alpha^2(\mu)$ rather than $\alpha(\mu)$. For moments ξ_F , this is equivalent to measuring the weighted average of $\alpha^2(\mu)$ over the window $F(\mu)$, whose expected maximum likelihood value we express as $\langle \alpha_F^2 \rangle$ and is somewhat simpler to interpret for some functions $F(\mu)$. In this case, we have that

$$\langle \alpha_F^2 \rangle = \int_0^1 d\mu F(\mu) [\mu^2 \alpha_{\parallel}^2 + (1 - \mu^2) \alpha_{\perp}^2]. \quad (7)$$

In the following we consider both approaches, fitting for either α_F or $\langle \alpha_F^2 \rangle$. Note that using a positive-definite function has the added advantage that, in real-space or post-reconstruction, the moments have the same shape as the linear 2-point clustering measurement

to first-order when $\alpha_{||} = \alpha_{\perp} = 1$. Thus they will all display a clear BAO feature that can be easily fitted.

Any single measurement of α_F or $\langle \alpha_F^2 \rangle$ from a moment of the correlation function or power spectrum will result in a degenerate measurement of $\alpha_{||}$ and α_{\perp} . Expanding around the best-fit solution to first order, we can fit the degeneracy direction showing that the primary measurement of α_F or $\langle \alpha_F^2 \rangle$ results in the same degeneracy, with a form

$$\alpha_F^{m+n} = \alpha_{||}^m \alpha_{\perp}^n, \quad (8)$$

where

$$m = \left. \frac{\partial \alpha_F}{\partial \alpha_{||}} \right|_{\alpha_{||}, \alpha_{\perp}=1} = \int_0^1 d\mu F(\mu) \mu^2, \quad (9)$$

$$n = \left. \frac{\partial \alpha_F}{\partial \alpha_{\perp}} \right|_{\alpha_{||}, \alpha_{\perp}=1} = \int_0^1 d\mu F(\mu) (1 - \mu^2). \quad (10)$$

The factor $m + n$ on the left-hand side of Eq. (8) renormalises α_F to the correct units.

In the following we consider particular forms for the function $F(\mu)$. The analysis should be valid for both power spectrum and correlation function analyses.

2.1 Fitting the monopole

For the monopole in real-space, $F(\mu) = 1$, and Eqns. (9) & (10) give that $m = \frac{1}{3}$ and $n = \frac{2}{3}$, and one recovers the well-known result that BAO fits to the monopole constrain $\alpha_F = \alpha_{||}^{\frac{1}{3}} \alpha_{\perp}^{\frac{2}{3}}$, whose corresponding distance is commonly called D_V . Note that, for measurements of the dilation scale parameterised by $\langle \alpha_F^2 \rangle$, the fit constrains a linear combination of $\alpha_{||}^2$ and α_{\perp}^2

$$\langle \alpha_F^2 \rangle = \frac{1}{3} \alpha_{||}^2 + \frac{2}{3} \alpha_{\perp}^2. \quad (11)$$

For the monopole of the power spectrum in redshift-space,

$$F(\mu) = \frac{(1 + \beta \mu^2)^2}{1 + \frac{2}{3} \beta + \frac{1}{5} \beta^2}, \quad (12)$$

including the increase in clustering amplitude driven by the Redshift-Space Distortions (Kaiser 1987). Here $\beta = f/b$, where f is the logarithmic derivative of the linear growth rate with respect to the scale factor, and b is a linear deterministic bias. Substituting this into Eqns. (9) & (10) and defining $A = 1 + \frac{2}{3} \beta + \frac{1}{5} \beta^2$, gives that

$$m = \frac{1}{A} \left(\frac{1}{3} + \frac{2\beta}{5} + \frac{\beta^2}{7} \right), \quad n = \frac{1}{A} \left(\frac{2}{3} + \frac{4\beta}{15} + \frac{2\beta^2}{35} \right). \quad (13)$$

For the SDSS-III BOSS (Dawson et al. 2013) CMASS galaxies, Samushia et al. (2014) measured $\beta = 0.34$, which translates to $m = 0.49$ and $n = 0.76$ suggesting that, to first order, the BAO-scale constraints from the monopole power spectrum measurement depend on $\alpha_F = \alpha_{||}^{0.39} \alpha_{\perp}^{0.61}$. As expected, an increase in the clustering strength along the los leads to an increased dependence on $\alpha_{||}$ in the resulting measurement.

Post-reconstruction, it is standard to ‘‘approximately remove’’ the RSD based on the estimate of the potential obtained, leaving a clustering signal whose amplitude is approximately independent of μ (e.g., Padmanabhan et al. 2012; Burden et al. 2014). Spherical averaging to give the monopole means that there is no β -dependent term, and the dependence of the monopole will revert to the real-space value. Note that in this case, or in real-space, all equations are valid for both the correlation function and the power spectrum.

2.2 Fitting power-law moments

The Legendre polynomials form an orthogonal basis and are the standard approach to measuring anisotropic clustering. However, using such bases, we can have $F(\mu) < 0$ for some μ , and consequently, the recovered clustering signal cannot be considered as a sum of the clustering signals in different directions (Eq. 6 no longer holds). The interpretation of these moments is therefore complicated as the BAO information is not compressible into a single stretch value.

This is not true if we instead consider the power law moments from which the multipoles are composed. For a power law moment of the power spectrum in redshift-space,

$$F(\mu) = \frac{\mu^p (1 + \beta \mu^2)^2}{(p+1)^{-1} + 2\beta(p+3)^{-1} + \beta^2(p+5)^{-1}}, \quad (14)$$

and

$$m = \frac{1}{p+3} + \frac{2\beta}{p+5} + \frac{\beta^2}{p+7}, \quad (15)$$

$$n = \frac{1}{p+1} + \frac{2\beta-1}{p+3} + \frac{\beta^2-2\beta}{p+5} - \frac{\beta^2}{p+7}. \quad (16)$$

When $\beta = 0$, or post-reconstruction with RSD removal, this reduces to constraining $\alpha_F = \alpha_{||}^{\frac{p+1}{p+3}} \alpha_{\perp}^{\frac{2}{p+3}}$, which is valid for both the correlation function and power spectrum.

Note that fits to $\langle \alpha_F^2 \rangle$ constrain a linear combination of $\alpha_{||}^2$ and α_{\perp}^2

$$\langle \alpha_F^2 \rangle = m \alpha_{||}^2 + n \alpha_{\perp}^2, \quad (17)$$

and a first order expansion as described above does not simplify the analysis. The degeneracy directions for $F(\mu) = 1, 3 \int_0^1 d\mu \mu^2$, and $5 \int_0^1 d\mu \mu^4$ are displayed with black dashed curves in Fig. 1. As p increases, the moments depend increasingly strongly on $\alpha_{||}^2$ compared with α_{\perp}^2 .

As the Legendre multipoles are simply linear combinations of power-law moments, the combination of the monopole and quadrupole will contain the same information as the combination of the monopole and the $p = 2$ power-law moment. Consequently, BAO fits to either the monopole and quadrupole or to the μ^0 and μ^2 moments will provide the same information and, similarly, including either or hexadecapole and μ^4 moment will add the same information.

2.3 Fitting Wedges

One could also consider setting $F(\mu)$ to be a top-hat function in μ , for example splitting the monopole into two components separated at μ_d . Such moments have been termed ‘Wedges’ (Kazin et al. 2012, 2013). Using a subscript ‘1’ for $F(\mu) = 1/\mu_d$ for $0 \leq \mu \leq \mu_d$, and a subscript ‘2’ for $F(\mu) = 1/(1 - \mu_d)$ for $\mu_d \leq \mu \leq 1$, one finds in real-space that

$$m_1 = \frac{\mu_d^2}{3}, \quad n_1 = 1 - \frac{\mu_d^2}{3}, \quad (18)$$

$$m_2 = \frac{(1 - \mu_d^3)}{3(1 - \mu_d)}, \quad n_2 = \frac{(2 - 3\mu_d + \mu_d^3)}{3(1 - \mu_d)}, \quad (19)$$

which give the coefficients for both the approximation for α_F of Eq. (8) and exact solution for α_F^2 given by Eq. 17.

Fig. 1 displays the degeneracy directions between $\alpha_{||}^2$ and α_{\perp}^2 for the two wedges split at $\mu_d = 0.5$ using red dotted curves. The

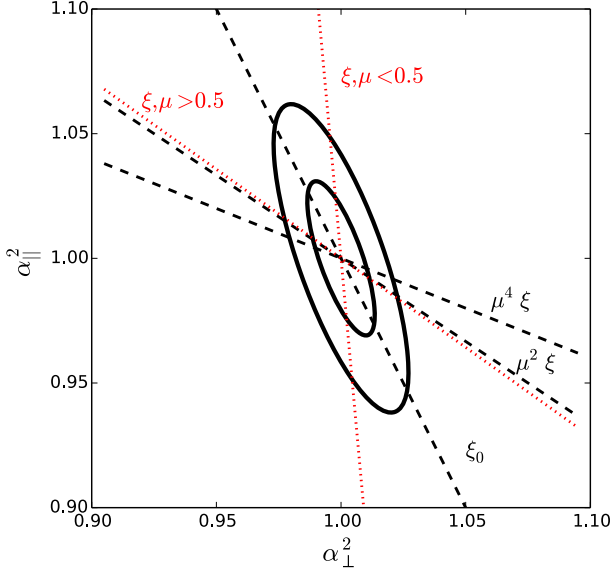


Figure 1. Straight-line curves denote the degeneracy direction between α_{\parallel}^2 and α_{\perp}^2 for various (single) clustering moments. Black dashed curves denote power-law moments $\int_0^1 d\mu \mu^p \xi(\mu) / \int_0^1 d\mu \mu^p$, which we denote $\mu^p \xi$, and red dotted curves denote Wedges. The solid ellipses denote the 1 and 2 σ contours for the optimal combination of two moments, as derived in the following section.

wedge with $\mu < 0.5$ constrains α_{\perp}^2 almost exclusively and the $\mu > 0.5$ moment has a similar degeneracy as the μ^2 power-law moment.

2.4 Fitting the Quadrupole

While the idea of measuring an average BAO position does not work with more general $F(\mu)$ models, the primary source of signal from the quadrupole is the strength of a feature proportional to the derivative of ξ_0 (see, e.g., Padmanabhan & White 2008; Xu et al. 2013). Therefore, in real-space, where there is no RSD, the amplitude of the BAO feature observed in the quadrupole carries the majority of the information on α_{\parallel} and α_{\perp} (as opposed to any other characteristic of the quadrupole). The amplitude of the quadrupole, relative to the underlying correlation function, depends on α_{\parallel} and α_{\perp} through

$$\frac{1}{\xi(r)} \left. \frac{\partial \xi_2(\alpha r)}{\partial \alpha_{\parallel}} \right|_{\alpha_{\parallel}, \alpha_{\perp}=1} = \frac{\partial \log \xi(r)}{\partial \log r} \int_0^1 \mu^2 (3\mu^2 - 1) d\mu, \quad (20)$$

$$\frac{1}{\xi(r)} \left. \frac{\partial \xi_2(\alpha r)}{\partial \alpha_{\perp}} \right|_{\alpha_{\parallel}, \alpha_{\perp}=1} = \frac{\partial \log \xi(r)}{\partial \log r} \int_0^1 (1 - \mu^2) (3\mu^2 - 1) d\mu. \quad (21)$$

The integrals in Eqns. (20) & (21) reduce to $\frac{4}{15}$ and $-\frac{4}{15}$ respectively, showing that the dependence on α_{\parallel} and α_{\perp} is equal and opposite, suggesting that the measurement will constrain

$$\frac{\alpha_{\parallel}}{\alpha_{\perp}} \frac{\partial \log \xi(r)}{\partial \log r}, \quad (22)$$

to first order, matching the dominant term in the expansion of Xu et al. (2013).

Table 1. BAO measurements on mocks as a function of μ . $\langle \alpha \rangle$ is the mean recovered stretch parameter (the relative BAO scale in that μ window), $\langle \sigma \rangle$ is the mean recovered uncertainty on α , and S is the standard deviation of the recovered α .

μ range	$\langle \alpha \rangle$	$\langle \sigma \rangle$	S	#
$0 < \mu < 0.2$	0.998	0.022	0.021	0
$0.2 < \mu < 0.4$	1.000	0.021	0.021	1
$0.4 < \mu < 0.6$	0.999	0.019	0.019	2
$0.6 < \mu < 0.8$	1.001	0.021	0.020	3
$0.8 < \mu < 1.0$	1.003	0.022	0.021	4

3 ERRORS ON MEASURED MOMENTS

If we can model the distribution of signal-to-noise of modes as a function of μ , we can predict the possible constraints one may obtain on α_{\parallel} and α_{\perp} . In redshift-space, on large-scales the modes have signal-to-noise that varies with μ , with the linear $(1 + \beta\mu^2)^2$ term increasing the amplitude of the power spectrum, which reduces the impact of the shot noise along the los. Although the amplitude of the modes are usually renormalised with the removal of the RSD during the reconstruction process, the signal-to-noise remains μ -dependent, as the ‘‘RSD removal’’ is effectively a renormalisation of the redshift-space modes, rather than a removal of signal (Burden et al. 2014).

The window function will also affect the signal-to-noise as a function of μ in the correlation function by varying the pair numbers, and in the power spectrum by reducing the number of independent modes. However, for samples such as BOSS CMASS, the window has a negligible effect, and the statistical distribution of pairs is close to being isotropic except on very large scales. On small scales, the BAO damping is asymmetric, and radial effects such as the Fingers-of-God (FoG) become important. Thus, we might expect the distribution of signal-to-noise to be a complicated function of μ .

We investigate the amount of BAO information as a function of μ empirically, using the methods described in Section 4, and the post-reconstruction mock catalogues for the BOSS CMASS sample, described in Section 5. We split the data into broad bins in μ and find the mean uncertainty and variance for BAO measurements in these bins. We present this information in Table 1, which shows that the BAO information is close to having an even distribution in μ for the correlation function. Minima for the recovered uncertainty and standard deviation on the measured BAO scale are found in the $0.4 < \mu < 0.6$ bin. A potential explanation is that between $0 < \mu < 0.5$ the effects of linear RSD boost the BAO signal, but at larger μ effects such as FoG remove information and reduce the signal-to-noise. Regardless, this minimum is shallow: the difference in recovered uncertainty is at most 15 per cent and the results therefore justify our choice to treat the information as constant in μ .

One may also worry about correlation between the clustering at different μ . For the power spectrum and an infinite volume, one expects no correlation between the clustering measured at different μ . Once a survey window is applied, correlations will be induced, but for a survey the size of BOSS we expect these correlations to be small at the BAO scale. We measure the correlation between the BAO measurements in the five μ bins described in Table 1 and we display the correlation matrix in Fig. 2. We find the magnitude of correlations is at most 0.15, and we expect the power spectrum

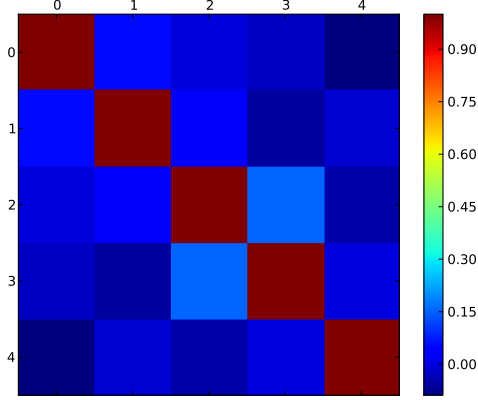


Figure 2. The correlation matrix of the five BAO measurements made in 0.2 thick μ bins obtained from 600 BOSS CMASS mocks, as described in Table 1 (and numbered in the same manner).

to be significantly less correlated than the correlation function. We therefore ignore any correlations between the BAO information at different μ in our analytical derivations that follow.

The results we presented in this section suggest that, to a good approximation, one can treat the distribution in μ of BAO information in the post-reconstruction DR11 BOSS CMASS sample as the same as that of an infinite real-space volume. However, the distribution for any given survey may vary based on the particular survey geometry, satellite velocities of the galaxy population (which smear the BAO feature at high μ), and the magnitude of the boost in clustering amplitude due to linear RSD effects (which boosts the high μ signal).

3.1 Complete sets of estimators

Suppose that we have measured $\alpha_{\text{meas},\mu}^2$ in a series of (independent) bins in μ (which we can treat as infinite in number), then fitting these measurements with parameters α_{\parallel}^2 and α_{\perp}^2 would minimise

$$\chi^2 = \int_0^1 d\mu \sigma_0^{-2} [\mu^2 \alpha_{\parallel}^2 + (1 - \mu^2) \alpha_{\perp}^2 - \alpha_{\text{meas},\mu}^2]^2, \quad (23)$$

where we have assumed that the value of $\alpha_{\text{meas},\mu}^2$ at a particular μ can be represented by a Gaussian random variable with expectation 0 and total variance σ_0^2 across all μ . Furthermore, we have assumed that the noise is evenly distributed in μ .

The maximum likelihood estimator for $(\alpha_{\parallel}^2, \alpha_{\perp}^2)$ can be calculated by finding the χ^2 minima, solving the equations $\nabla \chi^2 = \mathbf{0}$, where

$$\nabla \chi^2 = \frac{1}{15} \begin{pmatrix} 3 & 2 \\ 2 & 8 \end{pmatrix} \begin{pmatrix} \alpha_{\parallel}^2 \\ \alpha_{\perp}^2 \end{pmatrix} - \begin{pmatrix} \int_0^1 d\mu \mu^2 \alpha_{\text{meas},\mu}^2 \\ \int_0^1 d\mu (1 - \mu^2) \alpha_{\text{meas},\mu}^2 \end{pmatrix}. \quad (24)$$

Following Eq. (7), the measured value $\int_0^1 d\mu \mu^2 \alpha_{\text{meas},\mu}^2$ is a linear transform of that recovered from a moment of the 2-point function with $F(\mu) = 3\mu^2$, and similarly for the $F(\mu) = (1 - 3\mu^2)$ moment. Looking at both ‘‘measurements’’, we see that the maximum likelihood points are fully determined by the $p = 0$ and $p = 2$ power law moments, or equivalently by the monopole and quadrupole. Note that Eq. (24) relies on the fact that the model lin-

early depends on the parameters $(\alpha_{\parallel}^2, \alpha_{\perp}^2)$, and does not hold, for example, for fits to $(\alpha_{\parallel}, \alpha_{\perp})$.

Eq. (23) can also be written in terms of $(\alpha_{\parallel}^2, \alpha_{\perp}^2)^T$, with an inverse covariance matrix given by

$$C_{\alpha_{\parallel}^2, \alpha_{\perp}^2}^{-1} = \frac{1}{15\sigma_0^2} \begin{pmatrix} 3 & 2 \\ 2 & 8 \end{pmatrix}. \quad (25)$$

This can be calculated from the second derivatives of Eq. (23).

3.2 Predicted errors

In Section 3.1, we saw how the likelihood can be manipulated to understand constraints on α_{\parallel}^2 and α_{\perp}^2 from complete information (so the likelihood can be rewritten in terms of the new statistics), or the two $p = 0$ and $p = 2$ moments of those measurements. For fits to α_{\parallel} and α_{\perp} or for different moments, the likelihood derived is no longer complete. Instead, we recognize that for more general moments of positive-definite functions $F_1(\mu)$, $F_2(\mu)$ the covariance matrix is given by¹

$$\sigma_{1,2} = \sigma_0^2 \int_0^1 d\mu F_1(\mu) F_2(\mu), \quad (26)$$

and we use this formula throughout this section to determine the expected uncertainty on and covariance between α_{\parallel} and α_{\perp} when using clustering measurements for pairs of $F(\mu)$ windows.

For a general power law moment, $F(\mu) = (1 + p)\mu^p$, Eq. 26 yields $\sigma_p^2 = \frac{(p+1)^2}{1+2p} \sigma_0^2$. The covariance between an isotropic weighting and an arbitrary one is $\sigma_{0,F} = \sigma_0^2$. This implies that, in our formulation, introducing a measurement over a second window in μ as well as the monopole, does not provide extra information on the total stretch, it only provides a way to determine the radial and transverse components of the stretch.

Assuming a combination of measurements for $p_1 = 0, p_2 = p$, the radial and transverse stretch are given by (see Eqs. 9 and 10)

$$\alpha_{\perp} = \left(\alpha_0^{(3p+3)} \alpha_p^{-(p+3)} \right)^{\frac{1}{2p}}, \quad \alpha_{\parallel} = \left(\alpha_0^{-3} \alpha_p^{p+3} \right)^{\frac{1}{p}} \quad (27)$$

and we obtain the expected uncertainty on $\alpha_{\perp}, \alpha_{\parallel}$

$$\sigma_{\parallel}^2 = \sigma_0^2 \frac{p^2 + 8p + 10}{1 + 2p}, \quad (28)$$

$$\sigma_{\perp}^2 = \sigma_0^2 \frac{(p+13)(p+1)}{8p+4}, \quad (29)$$

and covariance $\sigma_{\parallel,\perp}$

$$\sigma_{\parallel,\perp} = -\sigma_0^2 \frac{p^2 + 2p + 7}{4p + 2}. \quad (30)$$

For $p = 2$, these equations reduce to the inverse of the matrix in Eq. (25). The variance and the correlation, $C_{\parallel,\perp} = \sigma_{\parallel,\perp} / (\sigma_{\parallel} \sigma_{\perp})$, are minimised for $p = 2$. Inspection of these results further reveals that they match those recovered in Section 3.1 for the optimal solution. Thus, we recover the same results using these approximate formulae as recovered for the (not approximate) ML solutions to measurements of α_F^2 , in the case where the ML solution is tested. We illustrate these results by plotting the 1 and 2σ contours predicted by these sets of covariances for $p = 2$ (black, solid), 4 (red,

¹ This is the general formula for covariance between the means of two Gaussian random variables with arbitrary $F(\mu)$ weighting and variance σ_0^2 for $F(\mu) = 1$. It does not depend on the definition of α or μ .

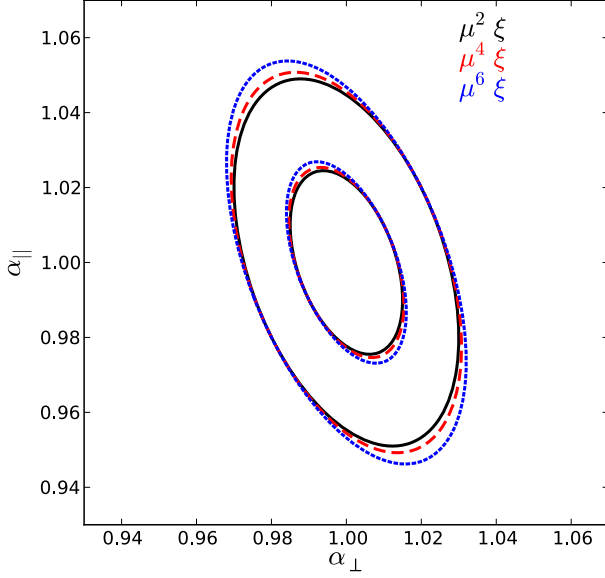


Figure 3. Ellipses showing the 1 and 2σ contours for α_{\parallel} and α_{\perp} , expected when combining the monopole with a power-law weighted moment $\int_0^1 d\mu \mu^p \xi(\mu) / \int_0^1 d\mu \mu^p$, which we denote $\mu^p \xi$, for $p = 2, 4, 6$ (black, red, blue).

dashed), and 6 (blue, dotted) in Fig. 3. The length of the minor axis stays nearly constant; which is in a similar direction to the measurement from the monopole (see Fig. 1).

For Wedges, Eq. (26) yields $\sigma_{1,2} = 0$ and $\sigma_1^2 = \sigma_0^2 / \mu_d$, $\sigma_2^2 = \sigma_0^2 / (1 - \mu_d)$. Given zero correlation between non-overlapping Wedges, in principle one may gain information by using an arbitrarily large number of (non-overlapping) Wedges. However, we have shown that just two moments, equivalent to the monopole and quadrupole, form a complete set estimators. Thus, we investigate only the case where two, non-overlapping, Wedges are used². We predict the uncertainties and covariance as a function of the Wedge split, μ_d , to be

$$\sigma_{\parallel}^2 = \sigma_0^2 \left(\frac{1}{\mu_d} \left[\frac{2\mu_d^2 + \mu_d^5 - 3\mu_d^3}{\mu_d^2(\mu_d^2 - 1)} \right]^2 + \frac{1}{1 - \mu_d} \left[\frac{3 - \mu_d^2}{\mu_d + 1} \right]^2 \right), \quad (31)$$

$$\sigma_{\perp}^2 = \sigma_0^2 \left(\frac{1}{\mu_d} \left[\frac{\mu_d^3 - 1}{\mu_d^2 - 1} \right]^2 + \frac{1}{1 - \mu_d} \left[\frac{\mu_d^2}{\mu_d + 1} \right]^2 \right), \quad (32)$$

and

$$\sigma_{\parallel, \perp} = \sigma_0^2 \left(\frac{(2 + \mu_d^3 - 3\mu_d)(\mu_d^3 - 1)}{\mu_d(\mu_d - 1)^2} - \frac{\mu_d^2(3 - \mu_d^2)}{(1 - \mu_d)(\mu_d + 1)^2} \right). \quad (33)$$

We evaluate Eqs. (31) and (32) for $0 < \mu_d < 1$ and compare the results to those recovered from the combination of α_0, α_2 (equivalent to the information in the monopole and quadrupole). The results are shown in Fig. 4. One can see that variance is minimized at $\mu_d = 0.64$, but that the α_0, α_2 combination always performs better. We display similar information in Fig. 5, except that we now plot the correlation $C_{\parallel, \perp}$. Its magnitude is also minimized

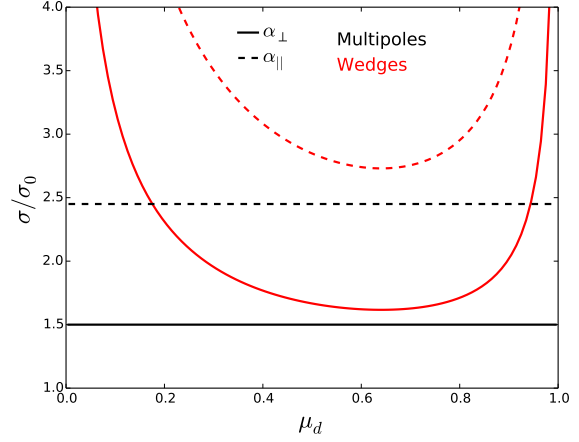


Figure 4. Red curves display the predicted uncertainty in α_{\parallel} (dashed) and α_{\perp} (solid) recovered using Wedges, as a function of the split in μ . The black curves display the predicted uncertainty for the combination of either the monopole and quadrupole, or the monopole and a μ^2 window.

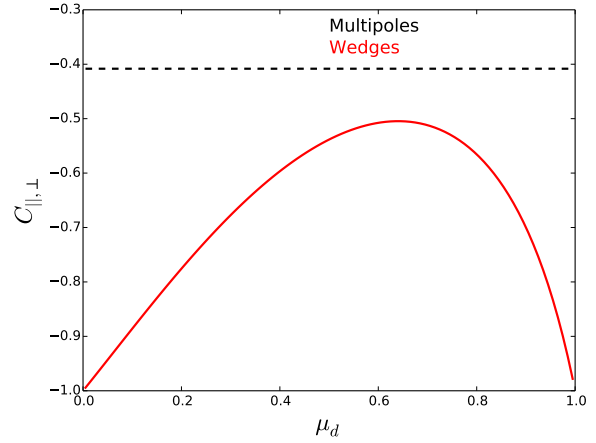


Figure 5. The solid red curve displays the predicted correlation between α_{\parallel} and α_{\perp} recovered using Wedges, as a function of the split in μ . The dashed black curve displays the predicted uncertainty for the combination of either the monopole and quadrupole, or the monopole and a μ^2 window.

at $\mu_d = 0.64$ and is always greater than that of the α_0, α_2 combination.

Table 2 summarises the predictions we make for the recovered uncertainty on $\alpha_{\parallel}, \alpha_{\perp}$ and its correlation. One can see that the predicted uncertainties on α_{\parallel} and α_{\perp} and their covariance are worse, by close to 10 per cent for each, for Wedges than for the combination of ξ_0 and ξ_2 . We illustrate this same information in Fig. 6, where the expected 1 and 2σ contours are displayed for Multipoles (black, solid) and Wedges split at $\mu_d = 0.64$ (red, dashed) are displayed. The major-axes of the ellipses are nearly aligned and it is along this direction that Wedges provide less-optimal constraints.

4 BAO FITTING

We use the same model to fit anisotropic BAO scale information as applied in Anderson et al. (2014). We use only post-reconstruction

² In the limit of infinite Wedges, the predicted uncertainties will clearly converge to that of the monopole and quadrupole

Table 2. The predicted uncertainty on the radial and transverse stretch, $\sigma_{||}$ and σ_{\perp} , relative to the uncertainty on the spherically averaged stretch, and their correlation, $C_{||,\perp}$. S denotes the standard deviation recovered from BAO fits to the mocks. $S_{||,\perp}$ denotes the correlation as recovered from the scatter of the BAO fits to the mocks. ‘W’ represents Wedges, and ‘M’ denotes the usage of ξ_0, ξ_2 . Compared to our predictions, the fits to the mocks are less precise but the overall trends agree. We discuss this further in subsequent sections.

Method	$\sigma_{ }$	σ_{\perp}	$C_{ ,\perp}$	$S_{ }$	S_{\perp}	$S_{ ,\perp}$
M	$2.45\sigma_0$	$1.50\sigma_0$	-0.41	$2.79\sigma_0$	$1.58\sigma_0$	-0.49
W, $\mu_d = 0.5$	$2.85\sigma_0$	$1.67\sigma_0$	-0.54	$2.98\sigma_0$	$1.73\sigma_0$	-0.56
W, $\mu_d = 0.64$	$2.73\sigma_0$	$1.62\sigma_0$	-0.50	$3.00\sigma_0$	$1.66\sigma_0$	-0.54

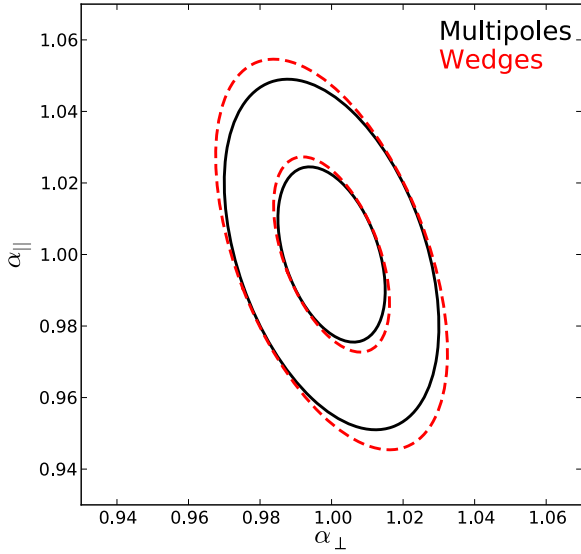


Figure 6. Ellipses showing the 1 and 2σ contours for $\alpha_{||}$ and α_{\perp} , expected when using multipoles (or μ^0 and μ^2 power-law moments; black) and when using Wedges split at $\mu_d = 0.64$.

data and match all fiducial parameter choices to those used in Anderson et al. (2014). We generate template $\xi(s)$ using the linear $P_{\text{lin}}(k)$ obtained from CAMB using the same cosmology as Anderson et al. (2014) (flat, $\Omega_m = 0.274$, $\Omega_b h^2 = 0.0224$, $h = 0.7$). We account for redshift-space distortion (RSD) and non-linear effects via

$$P(k, \mu) = F(k, \mu, \Sigma_s) \left(P_{\text{lin}} e^{-k^2 \sigma_v^2} + A_{\text{MC}} P_{\text{MC}}(k) \right), \quad (34)$$

where

$$F(k, \mu, \Sigma_s) = \frac{1}{(1 + k^2 \mu^2 \Sigma_s^2 / 2)^2} \quad (35)$$

and

$$P_{\text{MC}}(k) = 2 \int \frac{d^3 q}{(2\pi)^3} |F_2(k - q, q)|^2 P_{\text{lin}}(|k - q|) P_{\text{lin}}(q) \quad (36)$$

and we fix $\Sigma_s = 3h^{-1}\text{Mpc}$, $\sigma_v = 1.9h^{-1}\text{Mpc}$ and $A_{\text{MC}} = 0.05$ in all of our fits, as in Anderson et al. (2014). The motivation for these choices is discussed in Vargas Magaña et al. (2013).

Given $P(k, \mu)$, we determine the multipole moments

$$P_\ell(k) = \frac{2\ell + 1}{2} \int_{-1}^1 P(k, \mu) L_\ell(\mu), \quad (37)$$

where $L_\ell(\mu)$ are Legendre polynomials. These are transformed to ξ_ℓ via

$$\xi_\ell(s) = \frac{i^\ell}{2\pi^2} \int dk k^2 P_\ell(k) j_\ell(ks) \quad (38)$$

We then use

$$\xi(s, \mu) = \sum_\ell \xi_\ell(s) L_\ell(\mu) \quad (39)$$

and take averages over any given μ window to create any particular template:

$$\xi(s, \alpha_{\perp}, \alpha_{||})_{F, \text{mod}}(s) = \int_0^1 d\mu F(\mu') \xi(s', \mu'), \quad (40)$$

where $\mu' = \mu \alpha_{||} / \sqrt{\mu^2 \alpha_{||}^2 + (1 - \mu^2) \alpha_{\perp}^2}$ and $s' = s \sqrt{\mu^2 \alpha_{||}^2 + (1 - \mu^2) \alpha_{\perp}^2}$.

In practice, we fit for $\alpha_{\perp}, \alpha_{||}$ using ξ_0, ξ_2 and ξ_{W1}, ξ_{W2} , where $W1$ and $W2$ represent transverse and radial wedges split at either $\mu_d = 0.5$ or $\mu_d = 0.64$. When fitting to Wedges, we fit to the data using the model

$$\xi_{W1, \text{mod}}(s) = B_1 \xi_{W1}(s, \alpha_{\perp}, \alpha_{||}) + A_{W1}(s) \quad (41)$$

$$\xi_{W2, \text{mod}}(s) = B_2 \xi_{W2}(s, \alpha_{\perp}, \alpha_{||}) + A_{W2}(s), \quad (42)$$

where $A_x(s) = a_{x,1}/s^2 + a_{x,2}/s + a_{x,3}$.

To fit ξ_0, ξ_2 , we recognize $\xi_2 = 5 \int_0^1 d\mu (1.5\mu^2 \xi(\mu) - 0.5\xi(\mu))$ and, denoting $\int_0^1 d\mu \mu^2 \xi(\mu)$ as ξ_{μ^2} , we fit to the data using the model

$$\xi_{0, \text{mod}}(s) = B_0 \xi_0(s, \alpha_{\perp}, \alpha_{||}) + A_0(s) \quad (43)$$

$$\xi_{2, \text{mod}}(s) = 5 (1.5 B_{\mu} \xi_{\mu^2}(s, \alpha_{\perp}, \alpha_{||}) - 0.5 B_0 \xi_0(s, \alpha_{\perp}, \alpha_{||})) + A_2(s) \quad (44)$$

For all B_x , the parameter essentially sets the size of the BAO feature in the template. We apply a Gaussian prior of width $\log(B_x) = 0.4$ around the best-fit B_0 in the range $45 < s < 80h^{-1}\text{Mpc}$ with $A_x = 0$; this treatment assumes the amplitude of the BAO feature is isotropic.

5 EMPIRICAL RESULTS

We use PTHalo (Manera et al. 2013) mock galaxy catalogs (mocks) to empirically test our analytical derivations. The mocks we use were created to match the SDSS-III (Eisenstein et al. 2011) data release 11 (DR11) BOSS (Dawson et al. 2013) CMASS sample. The imaging (Fukugita et al. 1996; Gunn et al. 1998) and spectroscopic data (Smeed et al. 2013) were obtained using the SDSS telescope (Gunn et al. 2006) and reduced as described in Bolton et al. (2012)

The DR11 CMASS sample contains galaxies with $b \sim 2$ (White et al. 2011) distributed over 8500 deg^2 with $0.43 < z < 0.7$. The 600 PTHalo mocks created to match this sample are described in Manera et al. (2013) and Anderson et al. (2014). Results for Wedges and Multipoles fitting to these mocks have previously been published in Anderson et al. (2014), and we use the same post-reconstruction pair-counts as in Anderson et al. (2014). We bin $\xi(s)$ in s bins of width $8h^{-1}\text{Mpc}$, matching the fiducial choice of Anderson et al. (2014) that was determined optimal in Percival et al. (2014). We calculate $\xi(s, \mu)$ in μ bins of width 0.01 using the

Table 3. The statistics of BAO scale measurements recovered from the DR11 mock samples. ‘A14’ results are taken from Anderson et al. (2014). All values are recovered from the distribution of the fits to the 600 mocks; $\langle \rangle$ denote the mean values, S denotes standard deviation, and $C_{||,\perp}$ denotes the correlation between the maximum likelihood values of $\alpha_{||}$, α_{\perp} .

Publication	Method	$\langle \alpha_{\perp} \rangle$	$\langle \sigma_{\perp} \rangle$	S_{\perp}	$\langle \alpha_{ } \rangle$	$\langle \sigma_{ } \rangle$	$S_{ }$	$C_{ ,\perp}$
Anderson et al. (2014)	M	0.9999	0.0137	0.0149	1.0032	0.0248	0.0266	-
	W, $\mu_d = 0.5$	0.9993	0.0161	0.0153	1.0006	0.0296	0.0264	-
This work	M	0.9987	0.0150	0.0145	1.0017	0.0232	0.0257	-0.49
	W, $\mu_d = 0.5$	0.9992	0.0159	0.0157	1.0010	0.0274	0.0274	-0.56
	W, $\mu_d = 0.64$	0.9980	0.0153	0.0152	1.0032	0.0274	0.0276	-0.54

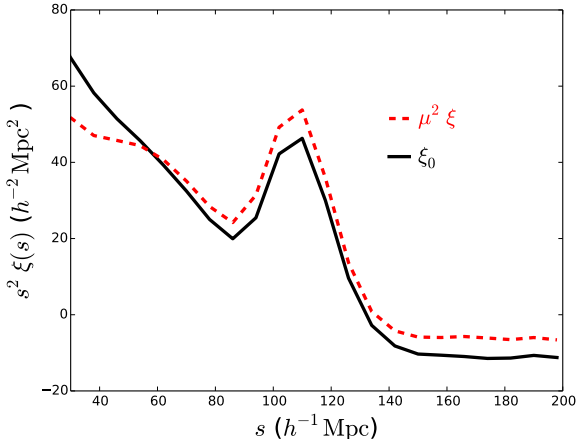


Figure 7. The mean ξ_0 and $3 \int_0^1 d\mu \mu^2 \xi(\mu)$, denoted $\mu^2 \xi$, recovered from post-reconstruction DR11 CMASS mocks.

Landy & Szalay (1993) method, modified for reconstruction (Padmanabhan et al. 2012),

$$\xi(s, \mu) = \frac{DD(s, \mu) - 2DS(s, \mu) + SS(s, \mu)}{RR(s, \mu)}, \quad (45)$$

where D is the reconstructed data points, R is a set of points randomly sampling the angular and radial selection functions, and S is a separate set of these random points whose positions have been shifted by the reconstruction according to the reconstructed density field (Padmanabhan et al. 2012). We then determine the correlation function for any particular window over μ via

$$\xi_F(s) = \sum_{i=1}^{100} 0.01 \xi(s, \mu_i) F(\mu_i), \quad (46)$$

where $\mu_i = 0.01i - 0.005$.

Fig 7 displays the mean ξ_0 recovered from these mocks post-reconstruction (black curve) compared to the mean $3 \int_0^1 d\mu \mu^2 \xi(\mu)$ moment (red curve). In principle, they should appear identical, as RSD have been removed in the reconstruction. However, differences are observed that are similar to the differences observed in post-reconstruction Wedges (see, e.g., figure 19 of Anderson et al. 2014).

We measure the line of sight, $\alpha_{||}$, and transverse, α_{\perp} , BAO scale information for each of the 600 mocks using three different pairs of observables:

(i) The combination of ξ_0 and ξ_2 , as described by Eqs. 43 and 44; we denote these results as ‘M’ (for Multipoles)

(ii) The combination of ξ_{W1} and ξ_{W2} Wedges split at $\mu_d = 0.5$; we denote these results as ‘W, $\mu_d = 0.5$ ’

(iii) The combination of ξ_{W1} and ξ_{W2} Wedges split at $\mu_d = 0.64$; we denote these results as ‘W, $\mu_d = 0.64$ ’

For both Wedges, we use the model described by Eqs. 41 and 42.

Our results are shown in Table 3, where we also display the results from Anderson et al. (2014), denoted with ‘A14’. One can see that our implementation of Wedges split at $\mu_d = 0.5$ and Multipoles generally match closely with Anderson et al. (2014), though variations of up to 10 per cent are found for some standard deviations and mean uncertainties.

The uncertainties and standard deviations are slightly worse than our analytic predictions, as can be seen by comparing the three left-hand columns to the three right-hand columns in Table 2. The discrepancies are greatest for $\alpha_{||}$ and for Multipoles; the recovered standard deviation on $\alpha_{||}$ is 14 per cent larger than expected for Multipoles, which is likely related to the fact that the correlation between α_{\perp} and $\alpha_{||}$ is 20 per cent larger than expected. Despite not matching our quantitative predictions, the Multipoles fits still match our qualitative predictions: they recover the smallest standard deviations, mean uncertainties, and correlation between $\alpha_{||}$ and α_{\perp} .

The Wedges split at $\mu_d = 0.5$ produce the results closest to our analytic predictions; the recovered α_{\perp} , $\alpha_{||}$, and their correlation are all between 3 and 5 per cent greater than predicted. We find that Wedges split at $\mu_d = 0.64$ results in only a small improvement in the variance of α_{\perp} and the correlation between α_{\perp} and $\alpha_{||}$ while producing a slight increase in the variance of $\alpha_{||}$. The $\mu_d = 0.5$ Wedges recover the least biased mean α_{\perp} and $\alpha_{||}$ of the three methods we apply, though the difference in the bias compared to the Multipoles results is negligibly small (at most 0.034σ).

The results of our fits to the mocks are illustrated in Fig. 8, where we take the standard deviations and correlations of $\alpha_{||}$ and α_{\perp} for the different fitting techniques we apply and assume Gaussian statistics. Compared to Fig. 6, one can see that the ellipses are all more elongated (reflecting the increased uncertainty on $\alpha_{||}$ over those predicted). Similar to our predictions, the Multipoles ellipse is significantly smaller than the Wedges ellipses.

Table 4 lists the correlations we find between the three different treatments we consider for $\alpha_{||}$ and α_{\perp} , and the standard deviation obtained when averaging the measurements accounting for the correlation. The correlations are all greater than 0.85, and differences from 1 are caused mainly by the relative precision achieved in each method. Thus, there is negligible gain achieved by averaging the measurements, as one can see that there is at best a one per cent gain in the precision over that achieved by using only the Multipoles results.

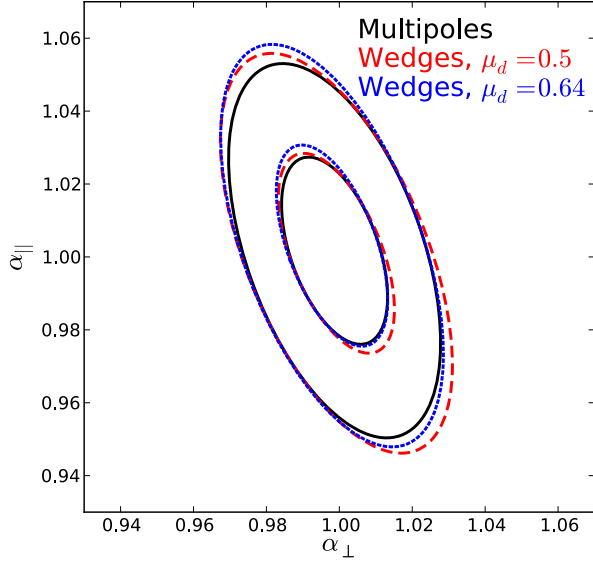


Figure 8. Ellipses showing the recovered standard deviation and correlations between the α_{\parallel} and α_{\perp} for the different fitting techniques we apply, produced assuming these statistics describe a multivariate-Gaussian likelihood distribution.

Table 4. Correlations between the recovered α_{\perp} or α_{\parallel} for different methods and the expected uncertainty when averages are taken incorporating the correlation. C denotes correlation and S_C denotes the standard deviation after combining the two measurements, accounting for the correlation.

Methods	C_{\parallel}	C_{\perp}	$S_{C,\parallel}$	$S_{C,\perp}$
Wedges $\mu_d = 0.5$; Multipoles	0.85	0.86	0.0254	0.0144
Wedges $\mu_d = 0.64$; Multipoles	0.89	0.90	0.0256	0.0144

6 CONCLUSIONS

We have derived analytic formulae that describe the relative importance of angular and radial dilation measured from moments of 2-point clustering statistics, with respect to the cosine of the angle to the line of sight μ . We have derived formulae for an arbitrary window, F , that weights information with respect to μ , and have provided solutions for the cases where $F(\mu)$ is a power-law (Section 2.2), a ‘‘Wedge’’ where $F(\mu)$ is 1 for given range of μ and zero otherwise (Section 2.3), and where the window is the 2nd-order Legendre polynomial (i.e., the clustering observable is the quadrupole moment; Section 2.4). We have presented results in real-space, valid for both the correlation function, and in Fourier space for moments of the power spectrum. These formulae extend the commonly used assumption that isotropically averaged BAO provide a measurement of $D_V(z)$ to other moments and allow for RSD when using power spectrum moments.

In Section 3, we derive the expected uncertainty of, and covariance between, α_{\perp} and α_{\parallel} obtained from a pair of clustering measurements calculated for two different $F(\mu)$ assuming that information is evenly distributed in μ (as is approximately the case for the BOSS CMASS galaxy sample). We show that the optimal, maximum likelihood solution is the combination of the monopole and quadrupole, or equivalently the monopole and $F(\mu) = \mu^2$. We show that a third power-law window only adds degenerate infor-

mation and should not increase the statistical precision on $D_A(z)$ and $H(z)$. We then find the optimal combination Wedges, which we find are those split at $\mu_d = 0.64$. For this optimal Wedge, we predict the uncertainties on and correlations between $D_A(z)$ and $H(z)$ are between 8 and 11 per cent larger than for the combination of the monopole and quadrupole.

Our results differ from those of Taruya et al. (2011); Kazin et al. (2012), as both studies found that including the hexadecapole significantly decreased the recovered uncertainty on $D_A(z)$ and $H(z)$. The key difference in our study is that we derive our results for post-reconstruction galaxy clustering measurements, where the Legendre polynomial moments are expected to be zero, except for the monopole. Thus, in our analytic formulation (supported by our empirical results), the inclusion of the quadrupole *does not* increase the total amount of BAO scale information (the covariance between the BAO information in the $p = 2$ moment and in the monopole is the same as the variance expected for the $p = 2$ moment), it simply allows for the information to be optimally projected into the $D_A(z), H(z)$ basis (and therefore *does* increase the total amount of cosmological information), and thus there is no additional information in the hexadecapole. In redshift-space, as studied by Taruya et al. (2011); Kazin et al. (2012), the quadrupole and hexadecapole are expected to be non-zero and thus do contribute to the total amount of BAO information.

In our derivations, we consider only the μ -dependent dilation at a particular scale and assume the information at particular μ is independent. Such an assumption may be more appropriate in k -space, where $P(k, \mu_1)$ and $P(k, \mu_2)$ are expected to be independent (not accounting for any survey window function), but we test our derivations using the redshift-space correlation function, where $\xi(s, \mu_1)$ and $\xi(s, \mu_2)$ are not independent. Despite these assumptions, the results we recover from test on mock samples closely match our predictions, especially for α_{\perp} , as presented in Section 5.

Using the set of mock catalogues produced for the BOSS DR11 analysis, we find that, as predicted, in terms of the recovered uncertainty of, standard deviation of, and covariance between α_{\parallel} and α_{\perp} , fitting to Multipoles produces the optimal results of the three cases we test, matching our analytic predictions. We also find, as predicted, Wedges split at $\mu_d = 0.64$ are optimal compared to Wedges split at $\mu_d = 0.5$, although the decrease in uncertainty is small (< 5 per cent). We find that the correlation between Multipoles and Wedges is large enough that there is a negligible gain in information (1 per cent reduction in the standard deviation) when the results are combined.

We find a slight trend where the methods that depend most strongly on clustering measurements at high μ are the most biased. The bias is small, as the largest bias, found for the $\mu_d = 0.64$ Wedge, is only 0.13σ . This trend is thus likely due to inaccuracies in our modelling of the BAO feature at high μ , where the non-linear RSD signal is strongest. If the modelling as a function of μ can be improved in future analyses, we expect the trend in bias will decrease and that the recovered uncertainties and correlations will be a closer match to our predictions for Multipoles. We therefore believe that improving the μ dependence of the post-reconstruction BAO template should be a priority for future BAO studies, and that by doing so, the precision of the measurements made using Multipoles will increase.

Our analysis provides further support for the future use of BAO to make robust cosmological measurements. We have carefully considered the meaning of BAO measurements made from moments of 2-point functions, providing an optimal approach. Both this work, and the recent work of Zhu et al. (2014) who considered

radial weighting of BAO measurements, are testing and optimising the BAO measurement methodology, increasing our understanding in line with the increasing statistical precision afforded by future surveys. Our results, and the conclusions we draw, are specific to the case where information is evenly distributed in μ . Thus, interesting possible extensions include extending the methodology to more general cases with different distributions of information with μ (e.g., $Ly\alpha$ or redshift-space measurements determined without using reconstruction), and allowing for correlations in μ in the covariance matrix of $\xi(\mathbf{r})$ required for small surveys. Such studies are likely to find that more than two moments are required to capture the full information content of the BAO signal.

ACKNOWLEDGEMENTS

AJR acknowledges support from the University of Portsmouth and The Ohio State University Center for Cosmology and AstroParticle Physics. WJP acknowledges support from the UK STFC through the consolidated grant ST/K0090X/1, and from the European Research Council through the Darksurvey grant. We thank the anonymous referee, Daniel Eisenstein and Nikhil Padmanabhan for helpful comments, Ariel Sanchez for comparisons with Wedges results, and Antonio Cuesta for providing all of the pair-counts we used in our mocks analysis.

Mock catalog generation and BAO fitting made use of the facilities and staff of the UK Sciama High Performance Computing cluster supported by the ICG, SEPNet and the University of Portsmouth.

Funding for SDSS-III has been provided by the Alfred P. Sloan Foundation, the Participating Institutions, the National Science Foundation, and the U.S. Department of Energy Office of Science. The SDSS-III web site is <http://www.sdss3.org/>.

SDSS-III is managed by the Astrophysical Research Consortium for the Participating Institutions of the SDSS-III Collaboration including the University of Arizona, the Brazilian Participation Group, Brookhaven National Laboratory, Cambridge University, Carnegie Mellon University, Case Western University, University of Florida, Fermilab, the French Participation Group, the German Participation Group, Harvard University, UC Irvine, Instituto de Astrofísica de Andalucía, Instituto de Astrofísica de Canarias, Instituto Catalana de Recerca y Estudis Avancat, Barcelona, Instituto de Física Corpuscular, the Michigan State/Notre Dame/JINA Participation Group, Johns Hopkins University, Korean Institute for Advanced Study, Lawrence Berkeley National Laboratory, Max Planck Institute for Astrophysics, Max Planck Institute for Extraterrestrial Physics, New Mexico State University, New York University, Ohio State University, Pennsylvania State University, University of Pittsburgh, University of Portsmouth, Princeton University, UC Santa Cruz, the Spanish Participation Group, Texas Christian University, Trieste Astrophysical Observatory University of Tokyo/IPMU, University of Utah, Vanderbilt University, University of Virginia, University of Washington, University of Wisconsin and Yale University.

REFERENCES

- Aihara, H., Allende Prieto, C., An, D., et al. 2011, *ApJS*, 193, 29
 Alcock C. & Paczynski, B., 1979, *Nature (London)* 281, 358
 Anderson, L., Aubourg, E., Bailey, S., et al. 2014, *MNRAS*, 441, 24

- Blazek, J., Seljak, U., Vlah, Z., & Okumura, T. 2014, *JCAP*, 4, 001
 Bolton, A. S., Schlegel, D. J., Aubourg, É., et al. 2012, *AJ*, 144, 144
 Burden, A., Percival, W. J., Manera, M., et al. 2014, *MNRAS*, 445, 3152
 Dawson K., et al., 2013, *AJ*, 145, 10
 Eisenstein D.J., et al., 2011, *AJ*, 142
 Eisenstein D. J., Seo H.-j., Sirko E., Spergel D., 2007, *Astrophys. J.*, 664, 675
 Eisenstein, D. J. 2005, *New Astr. Rev.*, 49, 360
 Fukugita, M., Ichikawa, T., Gunn, J. E., Doi, M., Shimasaku, K., Schneider, D. P., 1996, *AJ*, 111, 1748
 Gunn, J. E., et al., 1998, *AJ*, 116, 3040
 Gunn, J. E., et al. 2006, *AJ*, 131, 2332
 Font-Ribera, A., McDonald, P., Mostek, N., et al. 2014, *JCAP*, 5, 023
 Hamilton, A. J. S. 1992, *ApJL*, 385, L5
 Hu, W., & Haiman, Z. 2003, *Phys. Rev. D.*, 68, 063004
 Jeong, D., Dai L., Kamionkowski, M., Szalay, A.S., 2014, *MNRAS* submitted, arXiv:1408.4648
 Kaiser, N. 1987, *MNRAS*, 227, 1
 Kazin, E. A., Sánchez, A. G., & Blanton, M. R. 2012, *MNRAS*, 419, 3223
 Kazin, E. A., Sánchez, A. G., Cuesta, A. J., et al. 2013, *MNRAS*, 435, 64
 Landy S. D., Szalay A. S., 1993, *ApJ*, 412, 64
 Manera, M., Scoccimarro, R., Percival, W. J., et al. 2013, *MNRAS*, 428, 1036
 Padmanabhan, N., White, M. 2008, *Phys. Rev. D*, 77, 123540
 Padmanabhan, N., et al. 2008, *ApJ*, 674, 1217
 Padmanabhan, N., Xu, X., Eisenstein, D. J., et al. 2012, *MNRAS*, 427, 2132
 Percival, W. J., Ross, A. J., Sánchez, A. G., et al. 2014, *MNRAS*, 439, 2531
 Samushia, L., Reid, B. A., White, M., et al. 2014, *MNRAS*, 439, 3504
 Seo, H.-J., & Eisenstein, D. J. 2007, *ApJ*, 665, 14
 Smee, S. A., Gunn, J. E., Uomoto, A., et al. 2013, *AJ*, 146, 32
 Taruya, A., Saito, S., & Nishimichi, T. 2011, *Phys. Rev. D.*, 83, 103527
 Vargas-Magaña, M., Ho, S., Xu, X., et al. 2014, *MNRAS*, 445, 2
 White, M., Song, Y.-S., & Percival, W. J. 2009, *MNRAS*, 397, 1348
 White, M., Blanton, M., Bolton, A., et al. 2011, *ApJ*, 728, 126
 Xu, X., Cuesta, A. J., Padmanabhan, N., Eisenstein, D. J., & McBride, C. K. 2013, *MNRAS*, 431, 2834
 York, D.G., et al. 2000, *AJ*, 120, 1579
 Zhu, F., Padmanabhan, N., White, M., *MNRAS* submitted, arXiv:1411.1424